NTNU – Trondheim
Norwegian University of
Science and Technology

On the Design of Accurate Spatial and Temporal Temperature Measurements in Sea Ice

Karsten Meyer

Master of Science in Physics and Mathematics
Submission date: July 2012
Supervisor: Erik Wahlstrøm, IFY
Co-supervisor: Knut Vilhelm Høyland, Marin byggteknikk v/NTNU

Norwegian University of Science and Technology
Department of Physics

Abstract

Studies on sea ice have become increasingly popular among researchers in the last decades, due to its effect on the global climate and the challenges it presents for arctic engineering. The research is in demand of reliable data acquisition on various properties, in this case the temperature gradient in forming sea ice.

This project continues the development of a spatial temperature instrument, which intends to provide measurements with an accuracy of 0.01°C, making the researchers able to distinguish between fine variations in melting point due to salinity.

The outcome of the project is a complete revision of the probe design, which according to simulations not until now provides an environment for the sensor array that satisfies the accuracy requirement. The design also combines the low thermal resistance between sensor and medium from an earlier steel probe with the low thermal interference of an insulating plastic probe.

Manufacturing and assembly of the updated temperature instrument with a new probe is almost finished, and should after completion provide experimental data to back up the claims made by the simulations.

Sammendrag

Det har vært en økende interesse for forskning på sjøis de siste tiårene. Årsaken er isens innvirkning på det globale klimaet, og utfordringene den skaper for virksomhet i arktiske strøk. Forskningen er derimot avhengig av pålitelig innsamling av data, herunder temperaturmålinger for å undersøke gradienten i voksende sjøis.

Prosjektet tar for seg videreutviklingen av et temperaturinstrument til spatiale målinger som skal være nøyaktige ned til 0,01°C. En slik nøyaktighet gjør det mulig å skille mellom ulike saltnivåer og påvirkningen på smeltepunktet.

Resultatet er en revidert probedesign, som ifølge simuleringer først nå gjør det mulig å oppfylle kravet til målenøyaktighet. For øvrig kombinerer designen den lave termiske motstanden mellom sensor og medium fra en tidligere stålprobe, med den lave termiske forstyrrelsen fra en isolerende plastprobe.

Framstilling og montering av det oppdaterte temperaturinstrumentet med en ny probe er nesten fullført, og instrumentet bør kunne produsere eksperimentelle data som er i samsvar med simuleringene når det er operativt.

Preface

This paper constitutes the Master's Thesis for the writer, and is the conclusion of a five-year long Master of Science program in Applied Physics at the Norwegian University of Science and Technology (NTNU). It is the basis of evaluation in the course TFY4900 Physics at the Department of Physics. The thesis is a work of collaboration together with the Division of Marine Civil Engineering (MCE) at the Department of Civil and Transport Engineering (BAT), NTNU.

Professor Knut Høyland is the main supervisor from MCE, and has provided valuable insights in arctic research, which is the field of study in which this work will be applied. Associate professor Erik Wahlström has been the responsible supervisor from the Dept. of Physics. They have both offered their guidance in the process of documentation.

Emerited guest Bernt Førre at the Dept. of Physics has done most of the work regarding mechanical and electronic challenges. His remarkable knowledge in instrument prototyping has been key to complete this thesis. He has also given informal lecturing in topics ranging from programming to thermodynamics.

Frank Stæhli and Tage Westrum at the mechanical workshop at BAT have engaged in both the design work and the manufacturing of necessary hardware, and have as always provided a service of the highest quality.

Arne Moholdt at the Dept. of Physics and Harald Snekvik at The Faculty of Natural Sciences and Technology have assisted with some guidance when dealing with manufacturing challenges. Moholdt and Daniel Erland (BAT) have also done some of the ordering of materials not available at NTNU.

The project has in other words included contributions from a few people. The writer's tasks have changed somewhat in the process because of it. While originally partaking more in the practical execution, which due to illness and administrative difficulties have been delayed, the focus shifted toward a more computational aspect using simulations when there was a risk of not being able to obtain experimental data. Although the project was granted a one month postponement, it was not sufficient in order to complete the objectives. The delays have not been within the writer's control.

Given the nature of the project – a design process where the outcome inevitably changes along the way – the writer has in consultation with the supervisors decided to deviate from the standard IMRAD structure in this paper. The current layout attempts to link the content more clearly, while also giving a better idea of the chronological order of events.

Contents

Chapter 1

Introduction

There has been a rapid increase in arctic research in the last decades, with both economic and purely academic intentions. Discoveries of natural resources have made the Arctic an attractive region for oil companies, while also being a hot topic for climate scientists. Regardless of the purpose of the research, a recurring theme is the physics of sea ice.

Sea ice reflects radiation and acts as a heat insulating plate, and is therefore keeping the vast amount of water below it warm. The Arctic Ocean, which holds on average the largest reserve of sea ice on the planet, is thus an important contributor to the global climate. This makes analysis of the seasonal and yearly fluctuations of the sea ice levels in the Arctic important when studying climate changes.

Knowledge of sea ice mechanics is furthermore essential for arctic engineering, as any marine structure in the Arctic will be continuously surrounded by sea ice or experience drifting floes, and will as such require means of overcoming or enduring the ice.

The complications of sea ice follows from its perpetual solid-liquid transition, where it expels salt under formation whilst producing fresh water when it melts. Its thermal and mechanical properties will be affected by the embodied salt, whereas the expelled salt will produce a heavy saline that contributes to the convective mixing of the ocean.

The dynamic behaviour means that sea ice will have to be inspected in situ, where it forms naturally and is subject to e.g. the temperatures, impurities and salt levels it is normally found. This calls for field equipment capable of making accurate measurements of sea ice, without running a risk of breakdown due to

the extreme, arctic conditions. One of the desired devices is an advanced *temperature instrument* with spatial sensing capabilities, so as to make it possible to examine the temperature gradients in forming sea ice. Such a spatial device will also provide data on the ice thickness and growth rate.

Work on a digital instrument with a one-dimensional array of 15 temperature sensors was initiated by Egil Wille and Bernt Førre the fall 2009, as per request of professor in ice mechanics Knut Høyland. It is the aim of this thesis to continue the development of said instrument.

1.1 Requirements for measurements in sea ice

Several considerations must be made when developing measuring equipment for sea ice. If for instance the instrument generates a large amount of heat, it will raise the temperature locally so that the measurements do not correspond to the ice. Three main aspects to consider are:

- The instrument should not disturb the heat transport in sea ice from water to air, i.e. the instrument should not act as a thermal bridge. This would lead to an artificial change in temperature near the sensors.
- It should measure with a sufficient accuracy, designated at 0.01°C, thus enabling the scientist to distinguish between the fine variations in melting points due to salinity. The accuracy will furthermore need to be verified and documented through experiments.
- The instrument must endure the harsh conditions, so tolerating salt water and temperatures well below 0°C is essential.

1.2 Current status and present challenges

During the fall 2009 and spring 2010, Egil Wille and Bernt Førre made a few variations of a digital instrument with a probe containing 15 in-line temperature sensors [1, 2]. The intent was to "achieve a precision and accuracy of 0.01°C or better, and (...) to have a conversion time of 200 ms or less for each measurement" [1]. Such a requirement would ensure that the instrument would have been sufficiently accurate yet fast enough to be considered better than commercial instruments available at the time.

These versions had two different probe designs: One in a stainless steel casing, and another covered in a plastic heat-shrinkable tube. The design choices

have their benefits and drawbacks. A steel casing conducts heat well, allowing the instrument to respond quickly to temperature changes, but it will then interfere with the natural heat transport in the ice. A plastic fitting on the other hand insulates the probe, and so reduces its interference with the surroundings, at the cost of extending the response time of the measurements.

When this work was concluded in 2010, i.e. when Wille had finalised his thesis, the verdict was that the developed instruments satisfied the initial requirements. Subsequent use of the instrument has nevertheless indicated that the claim may be fallible, with the probes' thermal performances not living up to the accuracy of the measuring electronics. There was in other words more work to be done in order to finalise the development, and so it was resumed by the writer and Førre the fall 2011, during which the effort was directed at preparing a new probe design and implementing software.

For the spring 2012 and onwards, there are several key elements that need to be sorted out in order to present a useful and reliable field instrument:

- **The new probe design** needs to be manufactured, which involves hardware machining and electronics fabrication. Depending on the time available, the new probe will be one of two designs, whereof the most complex intends to combine the time response of the steel probe with the low interference of the plastic probe. In order to support any claim regarding the new probe's performance, there will be both acquisition of experimental data and thermodynamic simulations.

- **Updating electronics** where newer and improved components are available. This is particulary interesting where less noisy or quicker components will result in a better instrument.

- **Encapsulation** of the exposed electronics. The electronics that convert the analog readings to digital data and forward them to a host computer are currently not protected against the surroundings. For field use, there should be no risk of malfunction due to moisture or contact with salt water.

- **Wireless transmission** of the data communication between host computer and instrument. This would ensure that there are no difficulties regarding cabling other than the maximum wireless transmission distance.

- **Assembling the instrument** when a new probe, electronics and encapsulation are manufactured. The instrument has become more complex with every generation, and so combining all parts in the form factor the scientists want will be a challenge.

- **Calibration** is necessary to bring the developed instrument within the desired accuracy 0.01°C.

Chapter 2

Past work

Since this project is a continuation of previous work, we will need to outline the basic principles of operation for the former – and thus also the next – generation of the temperature instruments. A short introduction will give us a general idea of how the instrument functions, but will leave out some important details that can be investigated in the thesis by Wille [2]. Details relevant to the continued development will be elaborated upon.

In addition to the work presented by Wille, some experiments utilising both instruments were performed by Anders Lund Eide in spring 2011 [3]. Results highlighting the performance of the instruments are useful for stipulating the future aspects of development, depending on the possible weaknesses discovered by Lund Eide.

2.1 Principles of operation

The work done by Egil Wille and Bernt Førre is documented in detail by Wille in his reports [1, 2]. A quick walkthrough of the instrument might in any case be useful in order to understand the fundamentals. The instrument can be reduced to three main parts:

- A probe of 15 in-line temperature sensors at 10 mm intervals.
- An electronic interface with multiplexers (MUX), an analog-to-digital-converter (ADC) and a microcontroller unit (MCU).

- Software for the MCU that controls the multiplexers, collects the data from the ADC, and communicates with a host computer.

The instruments made by Wille and Førre can be seen in figure 2.1.

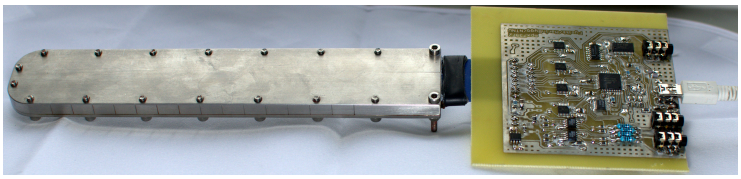

(a) Steel instrument

(b) Plastic instrument

Figure 2.1: Pictures of the two previous instruments.

2.1.1 Probe and sensors

Although the probe was designed with two different casings, the core is essentially the same in both. It consists of a printed circuit board (PCB) that connects a column of temperature sensors with the multiplexers in the electronic interface.

These instruments use thin film platinum temperature sensors, namely the Pt100 from Innovative Sensor Technology [4]. The Pt100 is a very accurate temperature sensor, with a polynomic relation between temperature and resistance. This relation may in addition be approximated to be linear, due to the diminutive contributions from the second and higher order of temperature in the region of interest [2, p. 10-11]. This results in the following function for the temperature:

$$T(R) = \frac{R - R_0}{R_0 A} \tag{2.1}$$

where T and R is the temperature and measured resistance, $R_0 = 100\ \Omega$ is the nominal resistance (hence the name Pt100), and $A = 3.9083 \cdot 10^{-3}\text{°C}^{-1}$ is the first order temperature coefficient. Error due to approximation is less than the

desired accuracy of 0.01°C for typical ice temperatures around 0°C, as explained by Wille [2, p. 11].

With a relation between temperature and electric resistance, it is possible to set up an arrangement for the sensors as seen in figure 2.2. By passing a current I through the loop, we use Ohm's law,

$$V = RI, \tag{2.2}$$

to compare the potential V_{ref} over a reference resistor, whose resistance R_{ref} is independent[1] of temperature, with the potential V_i over a sensor with resistance R_i. Since I is equal for all resistors in a series circuit, equation (2.2) gives the relation

$$\frac{V_i}{R_i} = \frac{V_{\text{ref}}}{R_{\text{ref}}} \Rightarrow R_i = \frac{V_i}{V_{\text{ref}}} \cdot R_{\text{ref}} \tag{2.3}$$

These sensors are mounted on a PCB with connections for the sensors using a spacing of 10 mm. In the stainless steel probe, the sensors are adhered to the steel casing with a thermal compound that ensures good thermal contact between the sensors and the steel casing. The steel wall with the glued sensors is much thinner than the rest of the casing with a thickness of only 0.7 mm, thus providing a short thermal distance between the sensors and the surroundings. An additional benefit of the thin wall is that it will not conduct as much heat *along* the sensing surface as it does *into* it [2, p. 14-15].

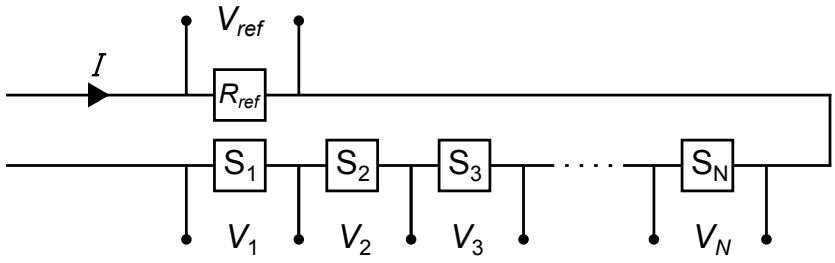

Figure 2.2: Scheme of the electronic setup in the probe. S_i and V_i are respectively the sensor and the potential across it at position $i = 1, 2, \ldots, N$. In this case we have $N = 15$.

[1] By *independent*, it is understood that the error due to temperature dependency is low compared to the desired accuracy. Although there are ultrastable resistors available on the market, they are expensive and will not give considerably better measurements.

The plastic probe consists of the same PCB strip with sensors, but without a sturdy casing around it. To protect the components, the probe is instead enclosed by a polyolefin[2] heat-shrinkable tube that is tightly shrunk around the electronics. The tube is coated with an adhesive on its inner wall, ensuring that everything stays in place and that the sensors have good thermal contact with the plastic. Plastic is on the other hand not a good thermal conductor, resulting in longer response times for the plastic probe than the steel probe [3, p. 46-47].

Regarding thermal disturbance, the steel probe has a severe issue in providing a conductive path between water and air, resulting in measurements that are not representative of the natural temperature gradient. The impact of the thermal interaction can be seen in the investigations by Lund Eide [3, p. 49]. It is much less of an issue for the plastic probe, being fitted with a thermally insulating material. In general, the disturbance leads to an artificial ice growth as displayed in figure 2.3.

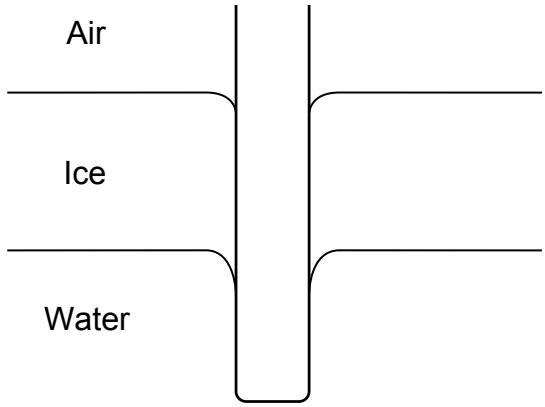

Figure 2.3: The result of having a conductive probe casing. It provides a thermal bridge between water and air, thus altering the temperature of the ice located at the casing. The thermal bridge's visual manifestation is the developing ice ridge along the probe at the ice/water intersection.

[2]A general term for polymers with olefin/alkene as the monomer, and includes common plastics like polyethylene and polypropylene. In practice we alternate between the terms polyolefin and plastic.

2.1.2 Electronic interface

In section 2.1.1 the principle of measuring the temperature at any given sensor has been established. In order to present sensible data to the user however, the measurements must be performed, processed and sent through a communication line to a host computer. Some extra hardware is required for the instrument to make this possible. As seen in figure 2.4, it includes:

- A set of multiplexers (MUX) that is connected to the sensor outputs in figure 2.2, and through external toggling outputs the desired sensor signal.
- An analog-to-digital converter (ADC) that receives the signal V_i from the MUXs, and compares it to the reference voltage V_{ref}.
- A microcontroller unit (MCU) that controls the MUXs, receives the signal from the ADC, calculates the temperatures by using equations (2.1) and (2.3), and forwards them to the user via USB.

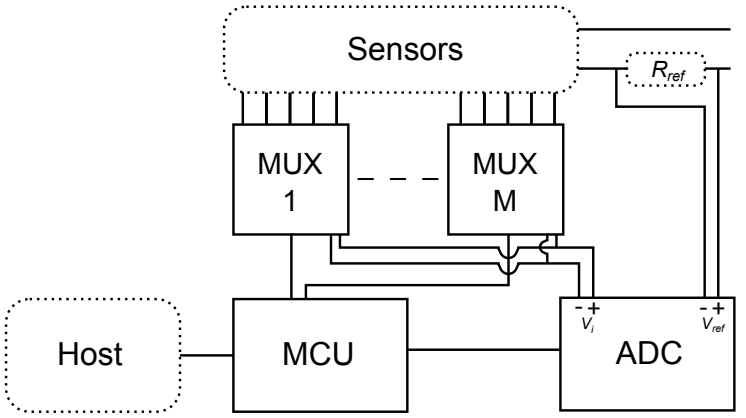

Figure 2.4: Simplification of the hardware that interfaces the sensors with a host. These instruments use 4-channel multiplexers, so that we need $M = 4$ multiplexers to switch between $N = 15$ sensors. The host is typically an ordinary PC, but could also be e.g. another MCU with logging capabilities.

This is however a simplification, as all of these components need some additional circuitry to perform as described. The ADC needs a buffer circuit, the

MCU needs an extra chip to communicate via USB, and there are a number of pull-up resistors and coupling capacitors controlling the currents. This project will not carry out radical changes to the interface, hence further details will be left unexplained. The main concerns are documented in depth by Wille [1, 2].

2.2 Software

There are two parts to the software for the instruments. Firstly, the interface electronics are operated by the MCU, as instructed by the software that is loaded into its memory. Secondly, the MCU also communicates with a host, and so the host has to understand the communication protocol and present the data to the user in an intelligible manner.

2.2.1 Instrument software

The software for the MCU was initially written in `BASCOM AVR`[3] by Wille to perform continuous measurements and write the data to the serial port. Wille's code featured a "bipolar" method of measurement [2, p. 20], indicating that every measurement was performed twice, e.g. from "left to right" and vice versa. By subtracting the negative voltage reading from the positive and dividing by 2, some errors in the multiplexing and conversion will be canceled out. This will of course increase the accuracy, but at the cost of doubling the time per measurement.

When the software was revised during autumn 2011, the instrument was given several modes of operation [5]. The user will now have to set the desired mode by passing a command byte to the instrument through the serial port, in accordance with the modes given in table 2.1.

As indicated in the table, the instrument has also been given the option of storing calibration vectors, so that every outputted temperature $\widetilde{T}_i$ at sensor i is given a positive calibration offset C_i from the measured temperature T_i:

$$\widetilde{T}_i = T_i + C_i \tag{2.4}$$

Previous instruments had an internal `EEPROM` of 2048 bytes, which is enough to store 10 separate calibration vectors without overwriting.

[3] A compiler by MCS Electronics that interprets a `BASIC`-derived language in order to produce fast and efficient machine code for AVR microcontrollers.

Table 2.1: List of the commands accepted by the instrument. Modes marked with asterisks will only affect how the measurements are performed.

Command	Mode
"U"	Unipolar*
"B"	Bipolar*
"S"	Single cycle
"C"	Continuous cycles
"Z"	Sleep
"X"	Device information
"G"	Get calibration
"M"	Modify calibration

2.2.2 Host software

As the communication between instrument and host computer got more complex, there was a need to develop host software that simplified the user's interaction with the instrument. Use of generic terminal programs, like `RealTerm`, demands great attention to underlying communication parameters, such as baud rate and control bytes. The dedicated software written in `Python` keeps these issues out of the user's scope.

The host software is divided into two parts [5]: An `IceLogger` module that tailors the `pySerial`[4] module to the temperature instruments, providing a user familiar with scripting with a `Python` object that controls all the functionality of the instrument. The user is thus given the opportunity to make scripts with custom logging routines.

The second part is a user interface based on `wxPython`[5] which utilises the aforementioned instrument module, giving the user a stand-alone program with buttons and menus that requires no specific computer knowledge to use. Through the `matplotlib` module, it can also make simple plots of previous log files. A screenshot of the program can be seen in figure 2.5a.

`Python` and the employed modules are all open source, and can thus be distributed freely.

[4] A community-written module for serial communication.

[5] A module that incorporates `wxWidgets`, a widget toolkit for cross-plattform graphical user interfaces.

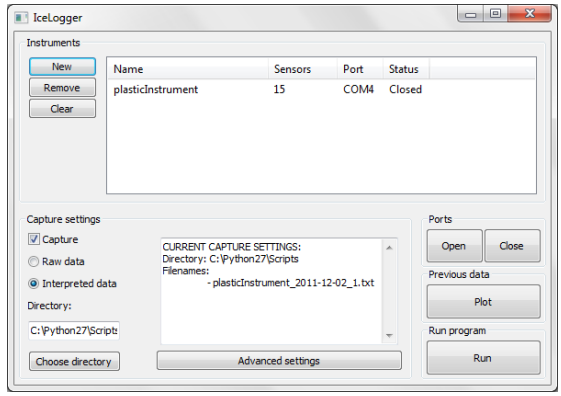

(a) Main window

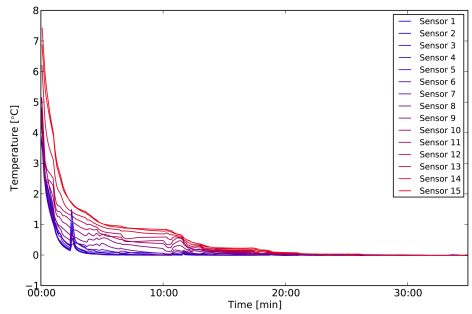

(b) Generated plot

Figure 2.5: The main window (a) of the user interface that can control one or more instruments. From here, one can connect, set the logging, and go to the "run" or "plot" windows. The program can generate plots like the one shown in (b), this one being taken from a calibration experiment with the plastic probe fall 2011 [5, fig 4.3a].

Chapter 3

Objectives

As outlined in section 1.2, there are still a few challenges to overcome before the instrument development is finished. We will not attempt to eradicate all issues in this project however, and will therefore concentrate on the main problem: Although the electronics behind the automated measurements are performing excellently, with a theoretical accuracy surpassing the instruments goal of 0.01°C [2, p. 40], we have shown that the thermal interference by the previous probes' hardware is of such magnitude that it affects the measurements. The previous steel probe for instance, has a severe issue regarding crosstalk, implying that the temperature at sensor i has an impetus on the temperature at its neighbours.

The primary obstacle in achieving a true accuracy of 0.01°C lies in other words in the performance of the probe that contains the sensors. Secondary challenges, such as preparing the instrument for the rough field use, will have to follow after the performance is verified.

Making a new, improved probe is thus the main objective. Verification of its performance will follow from experimental data and thorough thermal simulations, whereof both will provide information on the static and dynamic characteristics of the probe – i.e. what the offset is between medium and sensor temperature, and how quickly the probe responds to temperature changes.

Some effort will also be put in encapsulating the device, which is the next step after creating an improved probe. The new probe and its electronics will be of such a fashion that encapsulation is necessary to anchor the probe to the interface electronics.

Chapter 4

The cylinder probe

Both previous probes have an approximately rectangular cross-section. This would have been adequate if the probes had absolutely no thermal interaction with the surrounding ice. That is however not the case; there will always be some heat exchange, great or small, in such a manner that the instrument affects the natural temperature gradient between air and water. A rectangular probe will therefore disturb the ice growth anisotropically, thus rendering the temperature profile of the medium to be examined and measured unpredictable.

Although we want the heat exchange to be as small as possible, we could also attempt to make it cylindrically symmetric. This will in turn make the interaction homogeneous around the probe, so that the orientation of the sensing surface[1] is irrelevant. A cylindrical shape should be a good choice for the new probe, and the smooth surface of a cylinder should provide fewer irregularities for the forming ice to "grasp" onto (i.e. segments of space with lower temperatures), as has been the case with the corners and screw heads of earlier probes.

4.1 Mechanical layout

Independent of the shape, the probe will have to be based around a circuit board which contains all necessary electronic routings and sensors. The core is in other words a flat strip of PCB, around which there will be some hardware that forms

[1] No matter the shape of the probe, there will always have to be a surface section along the longitudinal axis where the sensors are mounted to the casing.

a cylindrical shape. Encompassing the PCB core with two cylinder halves should amount to a single cylindric unit.

The first design choice is thus the material of the cylinder halves. As indicated by the future user, ice researcher Knut Høyland, a low thermal disturbance is more desirable than a fast time response, so a thermally insulating material should be a fitting choice. Furthermore, it will have to be fairly stiff in order to produce a rigid probe. Polycarbonate (commercially known as e.g. "Lexan") rods are easily accessible in various sizes, with a thermal conduction similar to other plastics at approximately 0.2 $\mathrm{Wm^{-1}K^{-1}}$ depending on temperature and density.

They are however not very stiff; samples with diameters of 12 mm flex far too easily to form a solid probe. Less so for diameters of 16 mm, yet enough to require other means of reinforcement. Lexan cylinders of 16 mm diameters are nevertheless chosen as workpieces for the new probe as a compromise; the instrument should be as slim as possible, thus keeping the thermal mass small, and the 16 mm thickness will leave some room for reinforcing fasteners.

Two pieces of cylinder halves are made by grinding down a workpiece, so that the halves form a cylinder with a uniform radius together with a PCB core. To stiffen the probe and keeping the parts together, a set of 2.5 mm stainless steel screws are mounted radially in 20 mm intervals in the longitudinal direction. The principles of the design are illustrated in figure 4.1.

Each sensor measures 2.3 mm long and 2.0 mm wide [4], and will protrude from the core PCB. To accommodate these, we mill slots of 5 mm width in 10 mm intervals in the Lexan cylinder perpendicular to the PCB, as shown in figure 4.1a and 4.2.

With the internals being assembled as mentioned, we have a few options on how to seal the probe. An easy solution, which has already been tested on the plastic probe by Wille, is to enclose the entire cylinder in a heat-shrinkable tube. This will of course form the same thermally insulating barrier between the sensors and their surroundings as with the plastic probe. A more crafty solution is to also add thin metal caps over the sensors, and then punching holes in the tube at the sensor locations. The latter option should keep the thermal interaction between probe and medium fairly low, yet provide a short thermal distance between sensors and surroundings.

If the probe cylinder has a sufficiently uniform radius and a smooth surface, the tube can be shrunk without any air pockets. Getting the covering tube evenly shrunk is imperative, as the shrinking tube, which is coated with glue on its inner wall to make it adhere, will exert a mechanical stress to the internals if heated unevenly. Any strain in the copper traces to the sensors may cause electronic noise; the 24-bit ADC will pick up potential fluctuations as low as 2.7 μV [2,

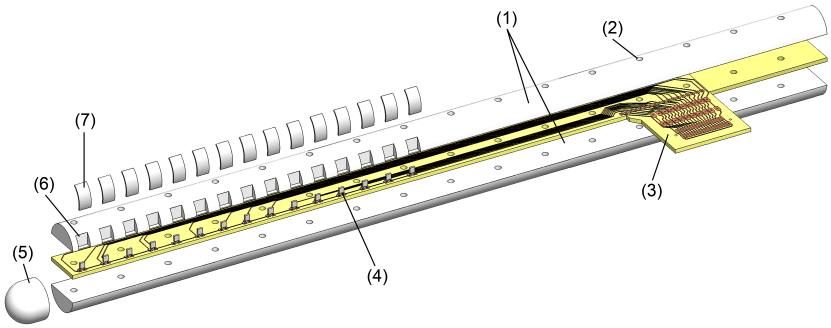

(a) Internals

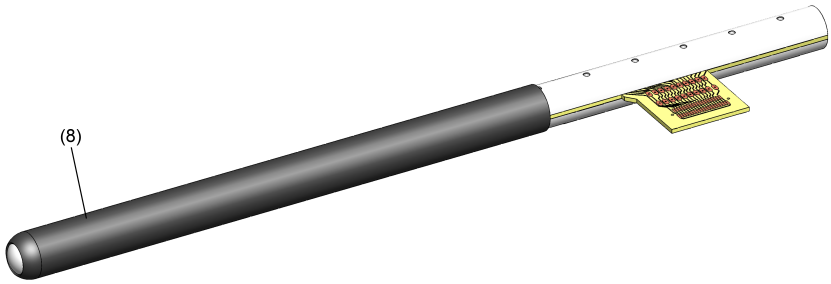

(b) Plastic version

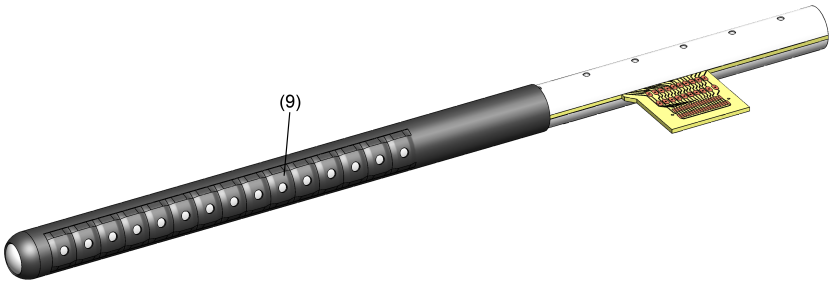

(c) Metal cap version

Figure 4.1: 3D models of the probe internals and the two differing casing designs. The internals consists of (1) Lexan cylinder halves, (2) screw holes, (3) PCB, (4) sensors, (5) an end piece, (6) sensor slots and possibly (7) metal caps. The casing is then (8) a polyolefin tube, with (9) punched holes for the metal cap version.

p. 12], and so the measurements are prone to all sources of noise, including those induced by mechanical stress.

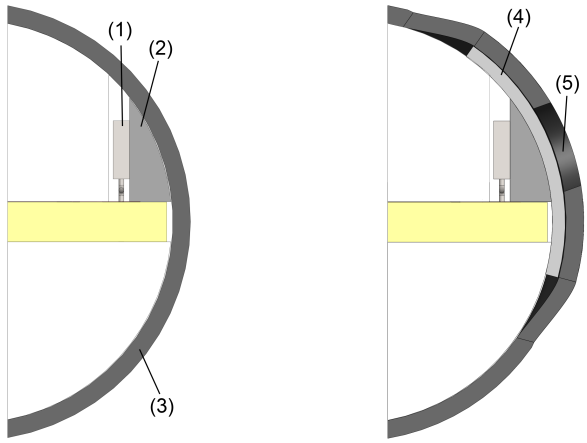

(a) Plastic version (b) Metal cap version

Figure 4.2: Cross-sections of the two probe designs. The sensors (1) are surrounded by thermal paste (2), making a thermal bridge to either the polyolefin tube (3) or metal caps (4). The punched hole (5) allows the metal to be exposed the external medium.

Which of the two options – with or without the metal caps – to adopt will depend on several aspects. First and foremost is the difficulty of assembly and the available time; it is important to get the punched holes located directly over the sensors, which may prove difficult with a shrinking tube coated with glue. The shrinkage will distort the shape, size and location of the holes, and the adhesive leaves no room for trial and error. Secondly, the thermal characteristics of the two options will have to be checked first, both through rough estimates and simulations of the heat transport.

4.2 Thermal considerations

As implied in figure 4.2, the sensor slots have to be filled with a compound that ensures a good thermal contact between the sensors and the probe cover. However, the requirements for such a compound, often called *thermal paste*, are quite strict. It will of course have to have a high thermal conductivity, yet be electrically insulating so as not to shorten the sensor wires. Furthermore it will have to

endure both very high and very low temperatures without deteriorating; it must not melt when applying heat on the heat-shrinkable tube, and similarily not crystallise when being used at sub-zero degrees. The *Boron Nitride Heat Sink Grease* from ITW Chemtronics [6] fulfills the criteria, with a thermal conductivity of 1.85 $\mathrm{Wm^{-1}K^{-1}}$ and a usable temperature range from $-73°\mathrm{C}$ to $200°\mathrm{C}$. The lower limit even surpasses the limit of electrical components at $-40°\mathrm{C}$. The thermal paste is also listed as nonconductive, with a dielectric constant of 2.2 at 100 Hz. However, by containing boron nitride and binding agents, the compound necessitates the enforcement of HSE rules regarding handling of chemicals (gloves, ventilation, etc.). The MSDS [6] lists potential health effects, such as "vomiting, acute abdominal pain and diarrhea" if ingested.

The metal cap version of the probe design requires finding a metal that performs well and is reliable, meaning that it conducts heat quickly into the thermal paste, yet withstands the corrosive conditions in salt water. Two such metals may be stainless steel and corrosion-resistant brass alloys, both available in sheets.

Rough estimates are useful for assessing general tendencies when accurate numbers are of lesser importance. For estimates of the conductive heat transport, e.g. when comparing different setups, Fourier's law[2] provides us with a useful relation for one-dimensional analysis,

$$\frac{\Delta Q}{\Delta t} = \kappa A \frac{\Delta T}{\Delta x}, \tag{4.1}$$

where $\Delta Q/\Delta t$ is the heat transfer rate, ΔT is the temperature difference at a length Δx, κ is the material's thermal conductivity, and A is the area through which the heat is conducted. Alternatively, we can insert $Q = \rho c T$, where ρ and c are mass density and specific heat capacity, into equation (4.1) and get

$$\frac{\Delta T}{\Delta t} = \frac{\kappa A}{\rho c} \frac{\Delta T}{\Delta x} \tag{4.2}$$

A rough estimate of the difference in the plastic versus metal design can be done by considering an instant where:

- The temperature difference ΔT between medium and thermal paste is the same.
- All heat is conducted through either the metal cap or the plastic tube, both with the same thickness Δx.

[2] A more stringent walkthrough of this is done in Chapter 5 - Simulations.

- The conductive area A is the same.

If so, the only difference in equation (4.2) for the two designs is the fraction $\kappa/(\rho c)$. Approximate values of these parameters are listed in table 4.1.

Table 4.1: Physical parameters for polyolefin tube, stainless steel and brass in rough figures [7]. Note that the polyolefin values are very general, and may be taken from similar polymers.

Parameter	Polyolefin	Stainless steel	Brass	Unit
κ	0.2	16	109	$\mathrm{W\,m^{-1}\,K^{-1}}$
ρ	950	7700	8500	$\mathrm{kg\,m^{-3}}$
c	2000	490	380	$\mathrm{J\,kg^{-1}\,K^{-1}}$

Computing the fraction $\kappa/(\rho c)$ for all cases, we have

$$\begin{aligned}\left(\frac{\kappa}{\rho c}\right)_{\text{tube}} &\approx 1.05\cdot 10^{-7}\ \mathrm{m^2/s}\\ \left(\frac{\kappa}{\rho c}\right)_{\text{steel}} &\approx 42.4\cdot 10^{-7}\ \mathrm{m^2/s}\\ \left(\frac{\kappa}{\rho c}\right)_{\text{brass}} &\approx 337\cdot 10^{-7}\ \mathrm{m^2/s}\end{aligned}$$

which illustrates the improvement in thermal performance that is available in adopting a metal cap design. Going from a pure plastic version to stainless steel caps, $\Delta T/\Delta t$ is increased in the region of a factor of 40, whereas brass caps yields a similar improvement of a factor of 320. Taken literally and neglecting all other factors, this implies that the time constant may be of a few orders of magnitude better when covering the sensors with metal rather than the insulating polyolefin. The estimate does not take into account the transported heat to or from the sensors through the probe internals (Lexan rods, circuit board and copper traces), which will alter the time response. This highlights the need for a more thorough analysis through simulation.

The improvement of the thermal bridge as explained above will also reduce the static offset between sensors and surroundings. When the instrument heading – interface electronics and encapsulation – is exposed to different temperatures than the probe casing, there will be a perpetual heat transport within the probe. Heat supplied to or withdrawn from the sensors through the probe internals and electronics will be dissipated/absorbed more efficiently through the steel or brass, thus reducing the equilibrium temperature difference between sensor and medium.

4.3 Electronics

As evident from figure 4.1, the PCB will feature an outlet for connecting the sensors to the interface electronics described in section 2.1.2 (see figure 2.4). The alternative to having an outlet is to make cuts in the Lexan cylinders, which would reduce the probe's stiffness. This gives us a bare section (without polyolefin tube) before and after the PCB outlet, which is supposed to be the anchor points for the enclosure that protects the rest of the electronics.

Circuit boards are made of prefabricated laminate sheets containing one or more layers of copper. The layers are stenciled and etched to form the conductive traces needed for the task. Laminate sheets for PCB production usually come as either single- or double-layered, indicating either a layer of copper on one or both sides of the sheet[3]. Sheets can be bought with 17.5 μm or 35 μm layers. We use 0.8 mm thick single-layered sheets with 17.5 μm copper thickness, giving us a small cross-section so as to minimise the heat conduction in the copper traces.

For a probe with $N = 15$ sensors, the PCB will contain 18 copper traces: 16 for measuring potential differences, and 2 to excite the sensor series with a current (see figure 2.2). With a 16 mm wide probe, and thus a 16 mm wide PCB, there is not much space for the traces and the required space between them. A trace width of 0.3 mm is the effectual maximum; the PCB will also have to accomodate holes for the reinforcing screws and some clearing between traces.

Since the instruments are still in the prototype stage, it is time-efficient to develop the PCBs using equipment available at hand rather than outsourcing the production to a professional supplier. The masks used for the development are printed on a transparent film, and the printers available have a pitch or resolution based on a round number of dots per inch (DPI). To get well defined traces, it is therefore viable to have a trace width that constitutes an integer amount of dots. Such dimensions could be 127 μm ($^1/_{20}$ in) or 254 μm ($^1/_{10}$ in).

Much of the heat conducted within the probe is transferred through the probe cylinder however. Comparing the probe cylinder to the copper traces using equation (4.1), assuming the same temperature difference in all components in the longitudinal direction, the heat conduction is dependent on the factor κA. Lexan and the PCB material FR4 share the same thermal characteristics with $\kappa \approx 0.2$ $\mathrm{Wm^{-1}K^{-1}}$, and together they form a cylinder of radius 8 mm. For a single copper trace of thickness 17.5 μm and either 127 μm or 254 μm width, and with a conductivity $\kappa \approx 400$ $\mathrm{Wm^{-1}K^{-1}}$, the factors κA are

[3]Sheets with 4, 6, 8 or more layers are also available to the industrial market, but require advanced machinery to process.

$$
\begin{aligned}
(\kappa A_{127})_{\text{copper}} &\approx 0.9 \cdot 10^{-6} \text{ Wm/K} \\
(\kappa A_{254})_{\text{copper}} &\approx 1.8 \cdot 10^{-6} \text{ Wm/K} \\
(\kappa A)_{\text{cylinder}} &\approx 40.2 \cdot 10^{-6} \text{ Wm/K}
\end{aligned}
$$

There are 18 traces going to and past the nearest sensor, of which 4 traces go to the furthermost sensor (2 for excitation and 2 for measuring). Using κA for 127 μm traces, the heat conducted in the copper accounts for approximately 8 % (furthest) to 29 % (nearest) of the total heat conduction within the probe at an instant where the temperature gradients of the cylinder and traces are equal[4]. Similarily, for 254 μm traces it ranges from 15 % to 45 %. This is of course rough figures, neglecting the impact of probe casing and fasteners, but it indicates that making the PCB with traces of 254 mm width will lead to a substantial – and reducable – heat conduction in the copper traces.

Trace dimensions as low as 17.5 μm $\times$ 127 μm could however lead to a generation of heat in the copper when passing current through it, to the extent that it interferes with the measurements. Through a curve fit to IPC-2221 [8], an excitation current of $I_{\text{ex}} = 0.7$ mA [2, p. 12] does not seem to be generating significant heat with traces of such dimensions, with the generated heat leading to temperature rises of a few tens of μK.

The concern when making traces as narrow as 127 μm is the quality of the traces. Microscopic cracks, gaps and other irregularites in the copper traces are difficult to avoid, as the print quality depends on the room temperature and humidity during fabrication. Film and printer cleanliness is also an issue, since any diminutive dust particles present when printing could break the conducting path. This is less of a challenge for 254 μm trace width; they will have twice the tolerance for such irregularites without breaking the conductor, and so it is much easier to develop high quality PCBs with wider traces. In the prototyping stage the project is in, we will therefore use 254 μm traces, which is still an improvement going from the 512 μm width in the former versions. A probe PCB with 254 μm traces can be seen in figure 4.3.

Regarding the electronic interface, which is connected the sensors via the connection pads on the outlet, the idea is to separate between the analog and digital circuitry. The sensor signals are all analog before the conversion, making them prone to noise sources. However, after conversion, all signals are digital and can be be transmitted to a separate PCB where all digital components are located. This will ease any further updates, whenever there is a desire to upgrade

[4]The difference in conductivity leads to different time constants, and so the temperature gradients will of course diverge shortly after.

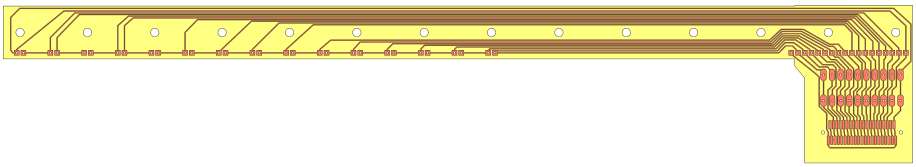

Figure 4.3: The printed circuit board in the probe, with 254 μm wide traces and an outlet for connections.

to e.g. wireless communication and newer microcontrollers – without having to interfere or replace the probe. For now, the interface electronics is a reshaped version of the previous interface, and is shown in figure 4.4. The figure shows that the interface is hold by the cylinder halves, which makes it necessary to add a dummy laminate sheet on the probe PCB up until the interface PCB, so that all sheets form a single unit of uniform thickness.

For intermediate testing, circuit verification, or even calibration purposes, it may also be interesting to have a detachable connection directly to the sensors. The outlet therefore features SMD pads for a 41-pin Harwin M40-620 [9], which guarantees a sturdy electrical connection with a maximum contact resistance of only 50 mΩ for up to 30 cycles of connect/disconnect. This will make it possible to check the probe circuit before assembling the instrument.

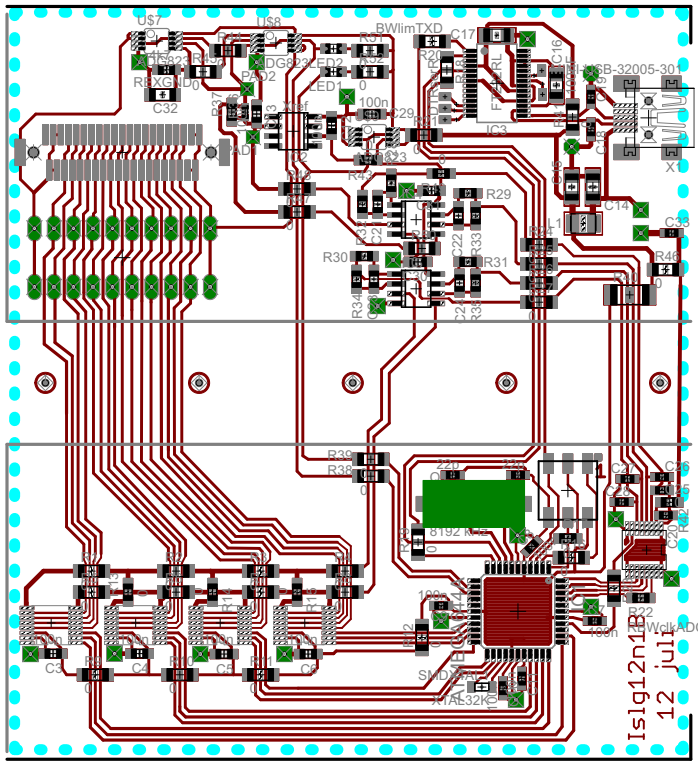

Figure 4.4: The reshaped interface electronics, which is mounted on the probe PCB and hold between the Lexan cylinder halves with holes for the reinforcing fasteners.

Chapter 5

Simulations

5.1 Theory

Simulation of the thermal response of various probe designs is a useful method of analysis, whether the aim is to select between differing design choices or validating the thermal properties. It is not a stand-alone tool however; regardless of the outcome of the simulations, some data and parameters will have to be set or corrected through comparison with experimental data.

It is in other words important to exercise caution when making bold statements based on simulation data. The reliability of said data is mainly dependent on the quality or accuracy of the model used when simulating. This includes both the mathematical representation of the thermal processes, and the shapes it is to be applied on.

5.1.1 Thermodynamics

When simulating the thermal response, we are in essence estimating the direction and magnitude of the *heat transfer* within and out of the instrument. We are not going to delve into the intricacies of thermodynamics, but the main principles of heat transfer are well known. The three common modes of transfer are:

- **Conduction** of heat between solids in physical contact.
- **Convection** of heat between solids and surrounding fluids.
- **Radiation** of heat through electromagnetic absorbtion or emission.

In addition to these, there is the possibility of heat transfer through mass transport, which is not applicable when analysing a stationary, solid object.

Conduction, which will constitute the heat transfer through the solids of the probe, is generally expressed by Fourier's law,

$$\boldsymbol{q} = -\kappa \nabla T, \tag{5.1}$$

where $\boldsymbol{q}$ is the heat flux [W/m^2] through an arbitrary surface $\boldsymbol{A}$, κ is the material's thermal conductivity, and T is the temperature. When studying heat transport however, equation (5.1) is commonly combined with conservation of energy to derive the *heat equation*[1],

$$\frac{\partial T}{\partial t} = \kappa \alpha \nabla^2 T, \qquad \alpha = \frac{1}{c_p \rho} \tag{5.2}$$

where c_p and ρ are respectively the specific heat capacity (at a constant pressure p) and the mass density of the solid. The solution to this partial differential equation, i.e. the temperature as function of position and time, will depend on the boundary conditions we apply for the system or domain. A boundary condition for the outer surface may be convective heat transfer with surrounding air or water.

The effect of such convection is normally estimated with Newton's law of cooling,

$$\frac{\partial Q}{\partial t} = hA(T_{\text{env}} - T), \tag{5.3}$$

with $\partial Q/\partial t$ being the heat transfer rate across a surface area A at temperature T, and h being the convective heat transfer coefficient of the surrounding fluid at temperature T_{env}. We can rephrase equation (5.3) by inserting $Q = c_p \rho T$, so that

$$\frac{\partial T}{\partial t} = h\alpha A(T_{\text{env}} - T). \tag{5.4}$$

The probe surface will also, by having a temperature $T > 0$ K, emit thermal radiation. The net radiative heat transfer rate has a strong temperature dependence,

$$\frac{\partial Q}{\partial t} \propto (T_{\text{env}}^4 - T^4) = T^4 \left(\left(\frac{T_{\text{env}}}{T} \right)^4 - 1 \right), \tag{5.5}$$

[1]The actual derivation of this partial differential equation is a common exercise in calculus or thermodynamics, and can be seen in e.g. [10]. Note that derivating it requires use of the relation for heat transfer rate: $\partial Q/\partial t = \boldsymbol{q} \cdot \boldsymbol{A}$, where Q is heat and t is time.

such that the radiative heat transfer is negligible when dealing with small deviations at low temperatures. The heat transfer between the solid probe casing and a surrounding fluid is thus mainly dependent on convection.

When solving the differential equation (5.2) including the given boundary conditions, we separate between a static and transient heat transfer state. For a static case, i.e. where the system is in its equilibrium, $\partial T/\partial t$ is zero at all positions, making the temperature a function of position alone. The solution to this case will highlight any temperature offsets between the surroundings and the sensors, whereas a transient analysis is useful to investigate the time response of the probe when exposing it to different temperatures.

5.1.2 Numeric approximations

Solving the three-dimensional heat equation with boundary conditions analytically would be far too complex for the irregular shapes of the probe, and thus we choose to do it numerically using the Finite Element Method (FEM). The idea is to slice a 3D model of the probe into a nodal network (a *mesh* or *grid*), where each node is the center of a volume element. The node contains all physical properties of its respective element, and will also interact with its nearest neighbour, meaning that heat will be conducted along the grid lines according to the heat equation.

A segment of such a nodal network is displayed in figure 5.1. This particular example is an isometric and cubic network, so that an (internal) node will exchange heat with the neighbours in x-,y- and $z-$direction. The node, at position (i,j,k), defines an element of volume $\Delta x \cdot \Delta y \cdot \Delta z$, where a quantity Δx is the distance between two nodes in the x-direction and so forth.

In a transient case, the aim is to be able to express an iterative process in time for every nodal temperature T_{ijk},

$$T_{ijk}^{(n+1)} = T_{ijk}^{(n)} + \Delta t \cdot \frac{T_{ijk}^{(n+1)} - T_{ijk}^{(n)}}{\Delta t}, \qquad \frac{T_{ijk}^{(n+1)} - T_{ijk}^{(n)}}{\Delta t} \xrightarrow{\Delta t \to 0} \frac{\Delta T_{ijk}^{(n)}}{\Delta t} \tag{5.6}$$

that can be solved for any time step n of length Δt. As indicated, the approximation in equation (5.6) is only reasonable for very small steps of length Δt. The equation raises an issue concerning the differentials in equation (5.2) and (5.4), which will then have to be approximated as finite differences.

First-order differentials $\partial T/\partial t$ are easily approximated as first-order differences $\Delta T/\Delta t$. An adaptation has to be made with the Laplacian,

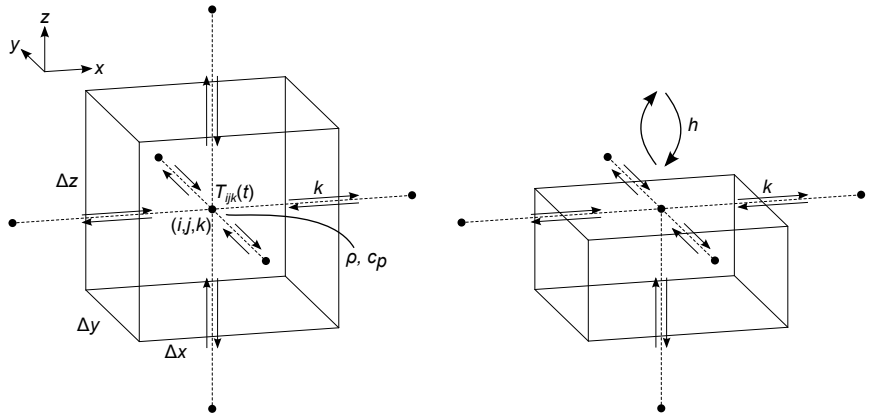

(a) Internal node (b) Boundary node

Figure 5.1: An internal and boundary node in a nodal network, shown with their corresponding volume elements.

$$\nabla^2 T = \frac{\partial^2 T}{\partial x^2} + \frac{\partial^2 T}{\partial y^2} + \frac{\partial^2 T}{\partial z^2}, \tag{5.7}$$

which has several numerical approximations, one of which is the second-order central difference, as suggested in the Crank-Nicolson method for solving partial differential equations [11]. The central difference states that

$$\begin{aligned} \frac{\partial^2 T}{\partial x^2} &\approx \frac{[T(x-\Delta x,y,z)-T(x,y,z)]+[T(x+\Delta x,y,z)-T(x,y,z)]}{(\Delta x)^2} \\ &= \frac{T(x-\Delta x,y,z)+T(x+\Delta x,y,z)-2T(x,y,z)}{(\Delta x)^2} \end{aligned} \tag{5.8}$$

which we can use to evaluate the Laplacian for a node at position (i,j,k), remembering that Δx is the distance between nodes in the x-direction etc.:

$$\left.\frac{\partial^2 T}{\partial x^2}\right|_{ijk} \approx \frac{T_{i-1,jk} + T_{i+1,jk} - 2T_{ijk}}{(\Delta x)^2} \equiv \delta_x^2 T_{ijk} \tag{5.9a}$$

$$\left.\frac{\partial^2 T}{\partial y^2}\right|_{ijk} \approx \frac{T_{i,j-1,k} + T_{i,j+1,k} - 2T_{ijk}}{(\Delta y)^2} \equiv \delta_y^2 T_{ijk} \tag{5.9b}$$

$$\left.\frac{\partial^2 T}{\partial z^2}\right|_{ijk} \approx \frac{T_{ij,k-1} + T_{ij,k+1} - 2T_{ijk}}{(\Delta z)^2} \equiv \delta_z^2 T_{ijk} \tag{5.9c}$$

Inserting equation (5.9) into (5.7), we establish the generalised notation for the central difference approach,

$$\nabla^2 T\big|_{ijk} \approx \delta_x^2 T_{ijk} + \delta_y^2 T_{ijk} + \delta_z^2 T_{ijk} = \delta^2 T_{ijk}, \tag{5.10}$$

which leads us to the final expression for the temperature changes due to heat transfer through conduction:

$$\left(\frac{\Delta T_{ijk}}{\Delta t}\right)_{\text{cond}} = \kappa_{ijk}\alpha_{ijk}\delta^2 T_{ijk}, \qquad \alpha_{ijk} = \left(\frac{1}{c_p \rho}\right)_{ijk} \tag{5.11}$$

Boundary nodes, on the other hand, will also transfer heat through convection with surrounding fluids in addition to the internal conduction. The exposed surface areas of the volume element for a boundary node will define the magnitude of the convection, in accordance with equation (5.4).

Boundaries will come in different fashions however, whether it is a corner node, an edge node or a planar node. Figure 5.1b displayed the latter, but for clarity we will examine the corner node in figure 5.2.

As suggested in the figure, a single volume element is comprised of octants, of which this corner node has seven solids and one fluid. The fluid octant reduces the surface area for the heat to conduct through to neighbouring nodes, e.g. from node $(i-1,j,k)$ to (i,j,k), and thus scales the heat conduction between them accordingly,

$$\delta_x T_{ijk} = \frac{\frac{3}{4}(T_{i-1,jk} - T_{ijk}) + T_{i+1,jk} - T_{ijk}}{(\Delta x)^2}, \tag{5.12}$$

where the factor $\frac{3}{4}$ stems from the reduction of conductive area[2].

[2]Although not immediately obvious from the heat equation (5.2), its derivation reveals that the heat transfer rate $\partial Q/\partial t = \boldsymbol{q} \cdot \boldsymbol{A}$ declines when the area is reduced.

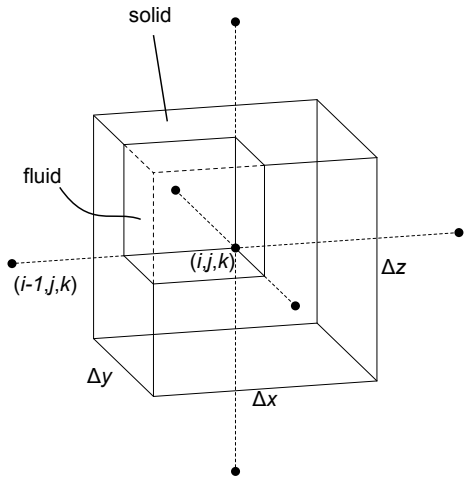

Figure 5.2: A corner node, which defines a volume that can be considered as 7 solid octants of which 3 are exposed to a fluid octant.

The fluid octant also exerts a convective heat transfer with the three neighbouring solid octants in the volume element. A single exposed octant will then have an exposed surface area of e.g. $\frac{\Delta x}{2} \cdot \frac{\Delta y}{2}$, and hence a total convective area for the element of

$$A_{\text{corner}} = \frac{1}{4}(\Delta x \cdot \Delta y + \Delta x \cdot \Delta z + \Delta y \cdot \Delta z), \tag{5.13}$$

from which it follows that the contribution to temperature changes due to convection is

$$\left(\frac{\Delta T_{ijk}}{\Delta t}\right)_{\text{conv}}^{\text{corner}} = h\alpha_{ijk}A_{\text{corner}}(T_{\text{env}} - T_{ijk}) \tag{5.14}$$

for a corner node at position (i,j,k). The effectual temperature changes for such a node will then be a sum of both the conductive and the convective contributions,

$$\frac{\Delta T_{ijk}}{\Delta t} = \left(\frac{\Delta T_{ijk}}{\Delta t}\right)_{\text{cond}} + \left(\frac{\Delta T_{ijk}}{\Delta t}\right)_{\text{conv}}, \tag{5.15}$$

which, for time step n, is inserted into equation (5.6).

5.2 Method

Implementing the numeric, thermodynamic formulae in section 5.1.2 on a modelled probe as described in chapter 4 is a task too strenuous to do from scratch; writing a program bottom-up to perform numeric analysis on a complex model according to the given formulae will consume more time than it is worth. There is already an abundance of commercial software available to both (a) construct a virtual model using a Computer-Aided Design (CAD) framework, and (b) perform thermal analysis on a given virtual model. Some software incorporates both aspects, such as `SolidWorks`. Although `SolidWorks` is an easy and intuitive CAD program, it is not very transparent in terms of the method of analysis, i.e. what goes on "under the hood". It is however compatible with other, and more specialised, software used for simulations such as `ANSYS`, which has an extensive documentation available for thermal analysis [12].

We can as such create a model of the probe in `SolidWorks`, and use it to define meshes, thus creating a nodal network, in such a manner that e.g. the small components are sliced in a fine mesh, whereas the larger components constitutes a more loose mesh. Furthermore, the program allows us to define the thermal contact points between components. `ANSYS` will then run the simulations accordingly, with the conductive and convective heat transport as explained in section 5.1.2.

Figures seen in chapter 4, that is figures 4.1-4.3, are all images of models built in `SolidWorks`, whereof the PCB in 4.3 is defined in the electronics program `EAGLE` first.

5.2.1 Model simplification

Ideally, we would be using the complex models illustrated in figure 4.1. However, meshing the fine elements and details in a satisfactory manner, that is without losing their shapes, would result in a large amount of nodes. The more nodes, the more degrees of freedom, and thus longer processing time for the CPU. The copper traces alone are long, yet so thin and detailed, that it would require nodes to the extent of hundreds of thousands degrees of freedom to be able to vaguely represent the traces. And even then we would gain a large error in e.g. their small conductive cross-sections, resulting in erroneus simulations. The various curved contact faces between components would require a similarily large amount of nodes to accurately resemble the correct contact areas.

As long as the simulations form a basis to discern between different design choices, i.e. as a tool of comparative analysis, employing a simpler model may

be reasonable as long as the general features are the same. This includes keeping the component volumes, contact areas and relations between components as similar to the complex model as possible. In other words, keeping the thermal masses of e.g. Lexan rods and copper traces, and the area of the exposed probe casing equal to the original model is imperative.

What we want to investigate is how the heat transported within the probe and through the casing affects the measurement. Other details, such as edge effects at the probe tip or what effects the cylindric geometry has on the medium are not the focal points of these simulations.

With that in mind, a way of simplifying the model is to change it to a rectangular "sandwich". Using only hexahedral shapes and flat contact surfaces makes it easier to assert that all component relations are maintained after meshing, and more importantly doing so at a managable number of elements. Adequate meshing of e.g. the curved shapes in figure 4.2 would require a very large amount of elements.

Simplified models of both the pure polyolefin and the metal cap version are made in `SolidWorks` as before, of which the metal cap version is shown in figure 5.3. Two slabs of polycarbonate encompass a single, wide copper trace. The slabs represents both the Lexan rods and the FR4-based PCB, which has similar thermal properties, so that they have the same volume as the original cylinder. In addition, the slabs and the trace maintain the exposed[3] area on the heading and outlet. The trace has the conductive cross-section of the 18 original traces with dimensions 17.5 μm $\times$ 254 μm to the first sensor, and is cropped down to 4 traces at the last sensor.

The polyolefin tube is represented by 0.7 mm thick slabs covering the lower exposed areas, also with the combined surface area as a cylinder of diameter 16 mm. For the metal version, it has slots for 0.5 mm thick caps at the sensor locations. The sensors are represented as protruding parts of the copper trace, with the sensing surface equivalent to the appropriate Pt100-sensors. Thermal paste connects the sensors to the overlying polyolefin or metal, retaining the fact that it will also be in contact with the polycarbonate. Stainless steel "screws" are lined up in 20 mm intervals, and have the same cross-section and length as the original 2.5 mm screws.

[3] "Exposed" in this context refers to the external, horizontal surfaces in figure 5.3.

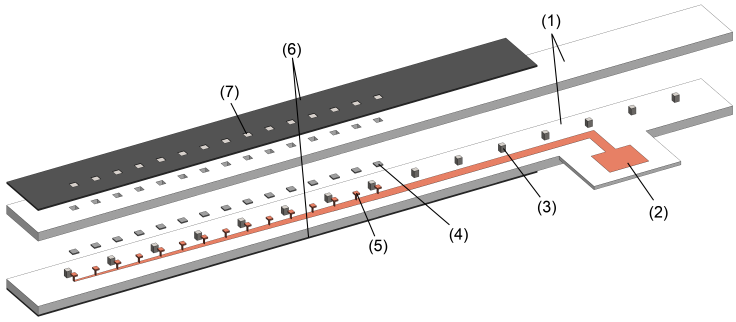

Figure 5.3: CAD model representing the simplified metal cap design. The numbering refers to (1) polycarbonate slabs, (2) copper trace, (3) stainless steel "screws", (4) thermal paste, (5) sensors, (6) polyolefin "tube", and (7) metal caps.

5.2.2 Preprocessing

After importing the geometry into ANSYS and defining all relevant material properties, the model needs to be prepared for the simulations. First off is checking all contact surfaces and if necessary correcting them; the autodetection employed by the software is based on setting a tolerance value for component spacing, which may or may not lead to lacking, redundant or otherwise erroneous contact zones.

How to mesh the model is arguably the biggest decision during preprocessing. Assessing the mesh quality is a matter of judgement and hard to specify in numbers. Generally speaking, the more elements the better the mesh. In practice, we have to make an educated guess at what regions are of most importance to the accuracy of the simulations, and then keep the total number of elements at a manageable amount. Figure 5.4 illustrates the resulting mesh. As seen in the figure, we also have a choice in the element shapes. The thin polyolefin "tube" is for instance easy to slice into hexahedral elements, while the larger polycarbonate slabs are represented by tetrahedrons that better preserve the contact with e.g. the stainless steel "screws" without increasing the element number. For the whole model, ANSYS uses 8 different element shapes, of which quadratic hexahedrons and tetrahedrons are the most frequent. Even for this simplified model, the total number of nodes approaches 129 000, whereof 65 000 are used to accurately represent the thin copper trace.

For transient analysis it is also important to tweak both the length of the time steps and the end time. Short time steps leads to more accurate simulations, but increases the number of iterations. For large temporal regions of interest, ANSYS

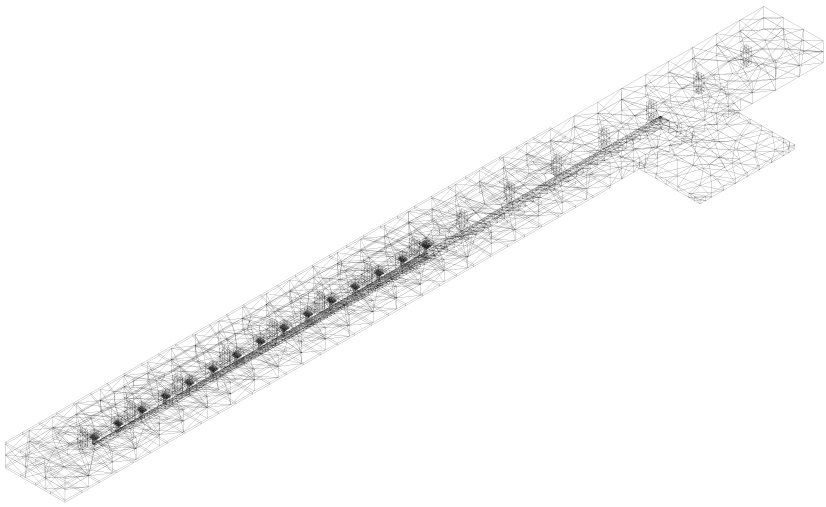

(a) The software's suggestion for the whole model.

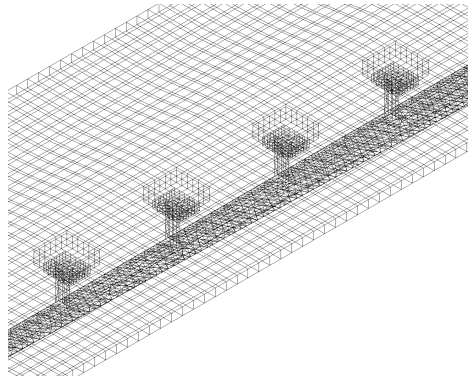

(b) Polyolefin "tube", metal caps, thermal paste, sensors and copper trace after refinement.

Figure 5.4: Depictions of the finite elements generated by meshing the simplified model in ANSYS.

allows us to divide the simulations into several steps: At the start, when the temperature changes are at its largest, we can have short time steps that increases towards the end time. Having time steps where the temperature changes are large, will accumulate to a margin of error that ultimately leads to an inaccurate simulation.

Finally, we set the simulation properties, such as excluding calculations and effects that are of lesser interest for our purpose, for instance the possibility to analyse *thermal strain effects*, which will lead to longer computation times.

5.2.3 Cases

Before having any experimental data from a finished version of the new probe design, the only references we have are the previous experiments conducted with earlier instruments. For the pure polyolefin design, i.e. without metal caps, the thermal response should be similar to the former plastic probe's response. This enables us to define a simulation case which resembles an experiment with the plastic probe, and then compare the corresponding performance of a metal cap design with the polyolefin version.

These simulations will therefore be based on the calibration experiments using the former plastic probe conducted the fall 2011 [5, p. 24-26] (see e.g. figure 2.5b). They are performed in a laboratory with an ordinary room temperature at, say, 22°C. The calibration medium, consisting of an ice/water slush mix, is fairly accurate at 0°C.

Transfering those conditions to our simulations in ANSYS, we are defining the boundary conditions as a fixed temperature of 22°C for the exposed surfaces of the probe heading, whereas the probe casing is applied a convective heat transfer with a medium at 0°C. The convective heat transfer coefficent h for this medium is of greater uncertainty, and is in general hard to estimate and varying with the fluid's and container's properties. For still water, it typically varies within a range of $20-100$ $\mathrm{Wm^{-2}K^{-1}}$ [7], but can approach 10 000 $\mathrm{Wm^{-2}K^{-1}}$ for a forced/flowing water sample. The calibration experiment was performed in a thermos with a still sample, but with occasional stirring for evening out any establishing, vertical temperature gradients in the slush. For the simulations, we have chosen convective heat transfer coefficients of 100, 200 and 400 $\mathrm{Wm^{-2}K^{-1}}$. Even though both heading and casing in real life would be exposed to convection with a fluid (water or air), we are fixing the temperature at the heading in order to reduce the number of simulation cases; for n different coefficients at the casing, we could certainly use n different coefficients for the heading, leading to n^2 combinations. This would only be a distraction; we are not interested in analysing the labo-

ratory conditions, and are therefore applying a worst-case scenario where the absorbed heat is at a maximum.

Having defined these boundary conditions, we choose three different cases for the simulations that will be interesting for the analysis:

- **Transient** response for the sensors when going from an initial, uniform temperature in the whole probe equaling that of the surroundings (22°C), to submerging the probe casing in a calibration medium at 0°C. This will highlight the difference in time response between the designs.
- **Static** temperature profile of the sensors for the equilibrium, i.e. when all temperature changes are set to zero. An offset between sensors and medium will highlight any limitations in measurement accuracy due to the probe hardware.
- **Crosstalk**, or smearing, between sensors when deliberately fixing the temperature of a sensor at a value different to the temperature the other sensors are exposed to, while performing the same static simulation as above. Such a case will reveal the degree of thermal dependency (or rather: the lack of *in*dependency) between the sensors.

These cases will all be simulated for a pure polyolefin casing, and a metal cap version using stainless steel or brass for the caps.

After every simulation, a result like the one displayed in figure 5.5 is outputted by the software, where one can insert *temperature probes* manually at any surface to extract and export the temperature data.

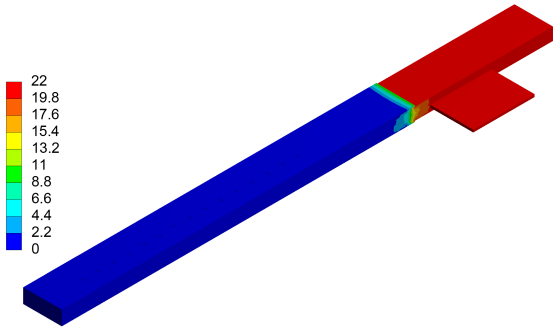

Figure 5.5: A sample contour colormap as presented after a thermal simulation.

5.3 Results

The following results refer to the three different simulation cases described in section 5.2.3. All results are gathered by probing and spatially averaging the temperature at the sensor surfaces of the described, simplified models. The accuracy requirement, set at 0.01°C, is marked in the plots where appropriate.

5.3.1 Transient response

Transient simulations for times up to 600 s are displayed for sensor 1 and 15 in figure 5.6. The labeling "h100" refers to using a heat transfer coefficient $h = 100\ \mathrm{Wm^{-2}K^{-1}}$ and so forth for the convective currents at the probe casing. The plots are cropped to better illustrate the differences between the polyolefin, steel and brass solution – all temperature lines start off at 22°C at $t = 0$ s, and decay to the temperatures shown in the plots.

The temperature progresses shown in the plots correspond well with exponential functions. Using any generic software to perform a curve fit, sensor 1 for polyolefin with $h = 100\ \mathrm{Wm^{-2}K^{-1}}$ in figure 5.6a yields

$$T(t) \propto \mathrm{e}^{-t/\tau}, \qquad \tau = 125.33\ \mathrm{s} \tag{5.16}$$

whose coefficient of determination $R^2 = 0.9993 \approx 1$ asserts that we have a good fit [13]. The exponential time constant for this sensor in this configuration is in other words $\tau = 125.33$ s.

To check the simulation data against the rough estimates presented in section 4.2, we also plot the time differentials for the stainless steel and brass cap models relative to the pure polyolefin casing. We define this quantity as the rate factor, RF:

$$\mathrm{RF} \equiv \frac{\dot{T}_{\mathrm{cap}}}{\dot{T}_{\mathrm{tube}}}, \qquad \dot{T}(t) \equiv \frac{\Delta T(t)}{\Delta t} \approx \frac{T(t+\Delta t) - T(t)}{\Delta t} \tag{5.17}$$

The resulting rate factors are plotted for the middle sensor, i.e. sensor 7, in figure 5.7. For figure 5.7b, the line representing $h = 100\ \mathrm{Wm^{-2}K^{-1}}$ for the brass cap version approaches 50 for $t = 0$ s. The simulations yield time differentials – at startup when the temperature differences between sensors and medium are equal – of a magnitude $10 - 15$ and $20 - 50$ times higher for stainless steel and brass compared to polyolefin, whereas the estimates proposed 40 and 320 respectively.

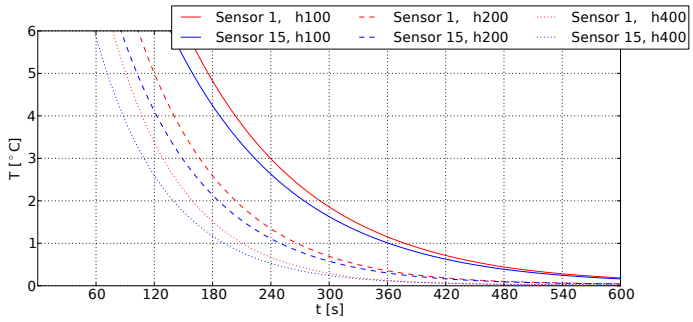

(a) Polyolefin

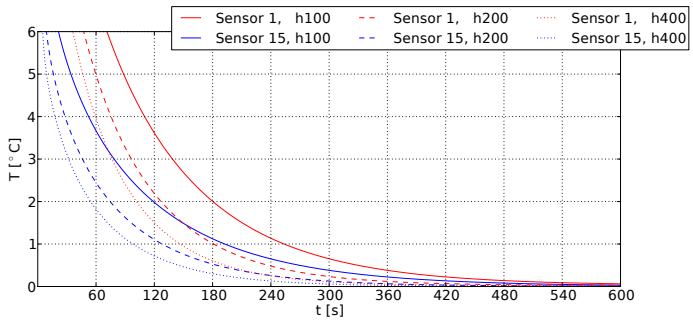

(b) Stainless steel

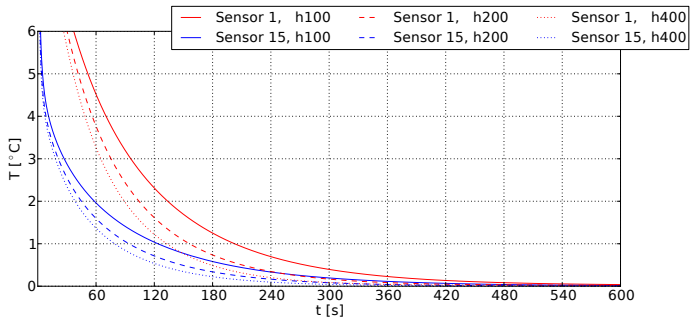

(c) Brass

Figure 5.6: Plots showing the temperature as function of time at sensors 1 and 15, for the convective heat transfer coefficients $h = 100$, 200 and 400 $\mathrm{Wm^{-2}K^{-1}}$.

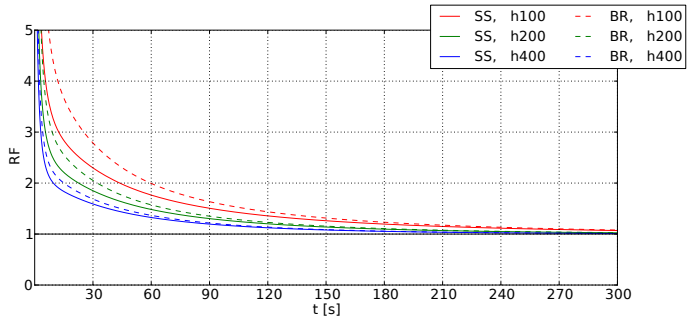

(a) $t < 300$ s

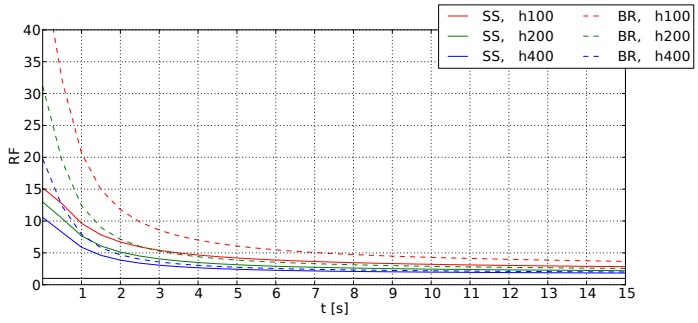

(b) $t < 15$ s

Figure 5.7: Plots of the rate factor RF for stainless steel caps (abbrev. "SS") and brass ("BR") at times $t < 300$ s and zoomed in at $t < 15$ s. The solid, horizontal line marks RF = 1. The plots are made for sensor 7.

5.3.2 Static offset

Static simulations showing the offset between the sensors and the medium at 0°C are plotted in figure 5.8. According to the plots, only the polyolefin casing has a severe offset issue for the first few sensors, with sensor 1 and 2 being outside the 0.01°C mark for these convection coefficients.

The plots are also showing some discrepancies among the sensors, with e.g. sensor 6 leveling out at lower temperatures than sensor 7 for all versions of the model. The steel screws are located at every odd sensor, so this may contribute to some variation between even- and odd-numbered sensors. Variations in the mK range represent fine variations in heat, so we may also be approaching the accuracy limitations in the simulations, coming from the actual modelling with inaccurate element representation of the model, and/or from the calculations with rounding and accumulated iterative residual errors.

5.3.3 Crosstalk

The same static simulations are performed as above, but with a fixed temperature of 1°C at sensor 7. Results are plotted in figure 5.9. The plots illustrate that the pure polyolefin design has a greater issue with crosstalk than the metal cap design, depending on the metal. For this particular setup, the crosstalk brings the 6 nearest neighbours out of the accuracy limit for the polyolefin, and similarily 4 or 2 for stainless steel and brass.

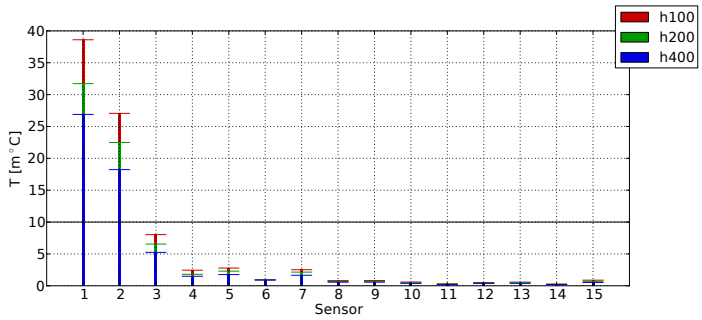

(a) Polyolefin

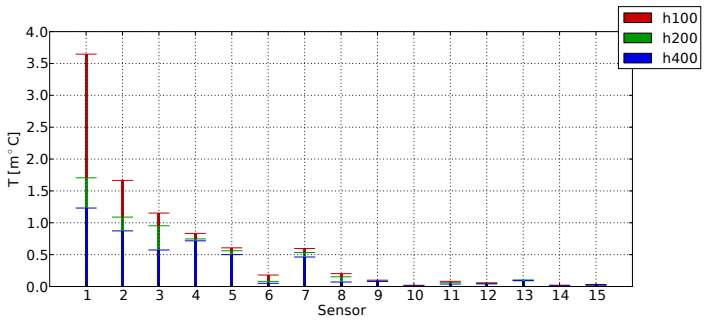

(b) Stainless steel

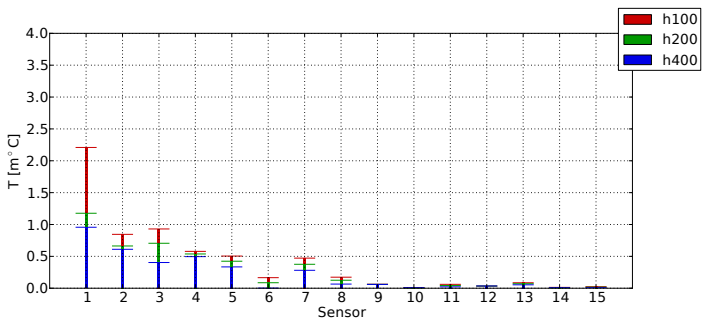

(c) Brass

Figure 5.8: Static offset between sensors 1 – 15 and surrounding medium at equilibrium. Note the different ordinate scaling for (a) compared to (b) and (c).

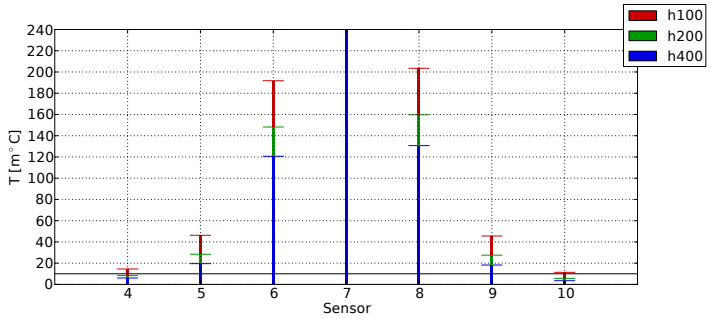

(a) Polyolefin

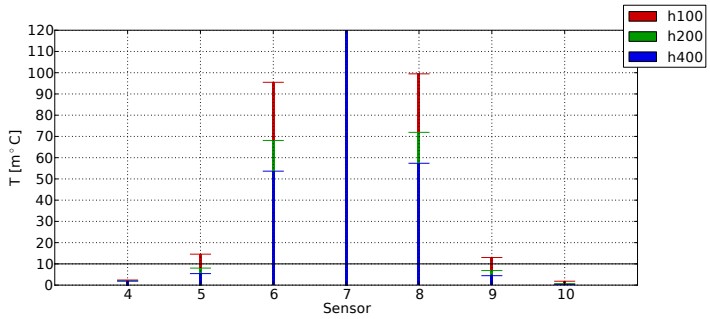

(b) Stainless steel

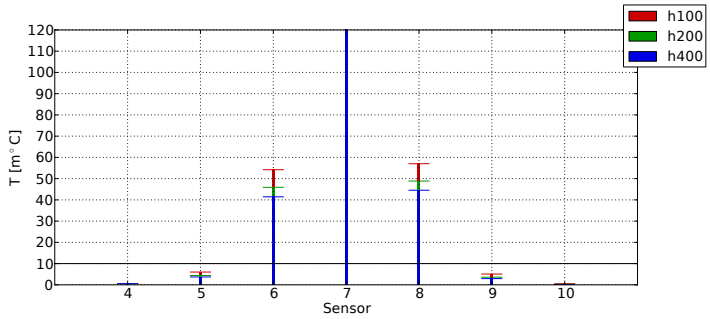

(c) Brass

Figure 5.9: Temperatures at sensors 4 – 10 when sensor 7 is fixed at 1°C.

Chapter 6

Manufacturing and assembly

Even though the general layout of the cylinder probe is described in chapter 4, some measures are set from a manufacturing perspective – as opposed to defining everything based on what may benefit the measuring system. The design process is in itself dynamic, with changes being made along the way according to comments from the workshop, feasibility regarding the production of electronics, and also depending on whatever challenges that arise during production.

6.1 Probe and electronics

By prototyping the electronics using equipment available at NTNU, we have a restriction in the maximum length for the probe PCB depicted in figure 4.3. The foil printer can handle the ordinary A4-format of 297 mm length, though it is good practice to allow for some top and bottom margins. However, the connecting outlet on the PCB must fit within an enclosure, reducing the maximum separation distance between the sensor array and interface electronics even more; because of the heat conduction from the interface electronics to the sensors through the copper traces, it is favourable to have a healthy distance between the first sensor and the outlet. The final configuration, with a PCB length of 270 mm, leaves around 9 cm between the first sensor and the connectors, comparable to the previous probes' headroom of $7 - 8$ cm.

During production of the probe PCB, which involves checking the full length

of all copper traces for gaps, it is evident that we have a comfortable margin for irregularities with the 254 μm trace width. The final batch of PCBs are therefore produced with downscaled traces near the sensors, going down to a 150 μm trace width at the nearest few centimeters. The intention is to create a thermal "bottleneck", reducing the conductive cross-section right before the sensors. A picture of the probe PCB with the downscaling is presented in figure 6.1.

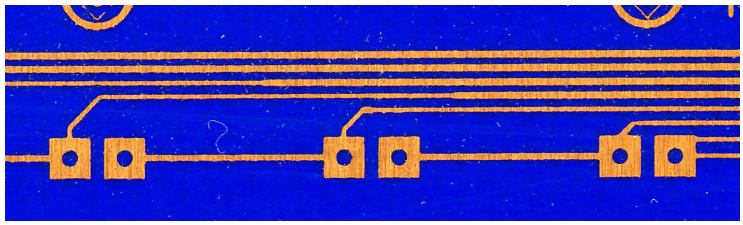

Figure 6.1: The developed probe PCB, with a principal trace width of 254 μm before narrowing it down to 150 μm before the sensors.

The grinding, cutting and milling of Lexan rods into cylinder halves are performed by the workshop in accordance with the dimensions given in section 4.1. They are manufactured with an ample length for potential adjustments when fitting it in an enclosure. A section of the prepared cylinder halves is shown in figure 6.2.

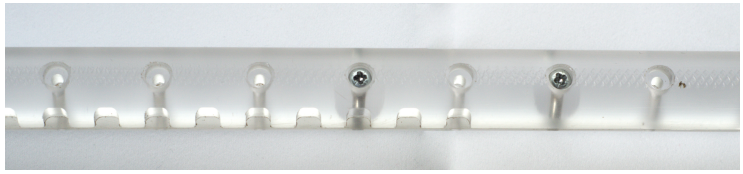

Figure 6.2: Close-up of the Lexan halves with milled sensor slots and screw holes. When assembling the probe, they will encompass the PCB with sensors and thermal paste in the slots.

For the casing, a polyolefin tube with a 19 mm inner diameter [14] fits perfectly around the 16 mm probe internals, and requires little shrinkage to form a tight bond. According to the datasheet, the tube wall should end up at around the same 0.7 mm thickness that is used in the simulations.

Regarding the slots, we make sure to bend the sensor terminals so that the sensors protrude towards the casing; the casing will push the sensors into the slots, and by overfilling the slots, any forming gaps will be taken up by paste, thus ensuring a short thermal path between sensor and casing.

Initial testing with the manufacturing of metal caps indicate that it may be difficult to assemble such a cap design. Press fitting bent caps onto the probe cylinder, where there can be small variations in curvature, causes a tension which may lead to movement and thus maybe a breach in the thermal contact. If so, the whole point with applying metal caps is lost as the thermal bridge between sensors and medium is ruined.

Altering the cap design by using thin metal film instead eliminates the issue with tension. Brass film of 150 μm thickness is cut into pieces with dimensions 8 mm $\times$ 14 mm, and bent to a curvature of 8 mm radius. However, such thin films are more prone to e.g. tearing, which is countered by covering them with polyimide Kapton tape [15] before assembly. The thin tape, with its thickness of just 69 μm and a thermal conductivity around 0.5 $\mathrm{Wm^{-1}K^{-1}}$, should not impose a significant thermal resistance to the system. Furthermore, taping the films to the probe cylinder before applying the heat-shrinkable tube eases the assembly process. The metal cap version is certainly feasible with this procedure – even at the prototyping stage.

However, with a lot of the manufacturing and assembly being performed in the completion phase of the project, a fully operational instrument utilising the new probe is not completed. Most parts are fully prepared, including the cylinder halves, probe PCB, metal caps, interface electronics and so forth, but assembling everything together and uploading the software still remains.

6.2 Encapsulation

With the way the probe and its electronics are shaped, with a cylindric construction and a small outlet for connections, the instrument will need an enclosure that anchors the probe to future, split interface PCBs in order to form a rigid unit. A watertight enclosure will of course also protect the electronics against salt water and impacts during field use.

The requirements for such an enclosure have already been investigated [5, p. 11-13], and the 1555 “F” enclosure from Hammond Manufacturing [16] is chosen for its listed applications. The manufacturer claims that it is “designed for harsh industrial environments or outdoor applications”, and it comes with internal mounting tabs for mounting the hardware within it.

The enclosure, as it is processed by the workshop, is depicted in figure 6.3. As shown in the photograph, the workshop has tailored a polyacetal nozzle and a clamping device to the enclosure, thus establishing two fixing points that hold the probe firmly in place. The nozzle allows us to have a spacious entering point for the probe in the enclosure, making it possible to thread the probe through at an angle before fixing it. While a gasket seals the opening between nozzle and enclosure, another heat-shrinkable tube can seal the nozzle and probe connection.

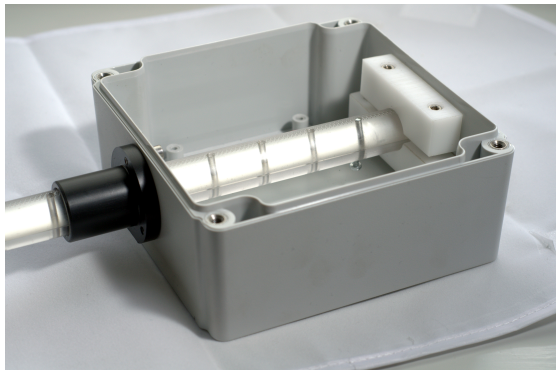

Figure 6.3: The prepared enclosure with a dummy Lexan cylinder. The clamp is fixing the cylinder to the back wall, whereas a nozzle at the front wall holds the probe and seals the enclosure with a gasket.

Although this configuration will hold all components together and keep the electronics protected from the surroundings, there is also a concern regarding the contained humidity. Sealing the enclosure at any given temperature and relative humidity, and then using the instrument in other conditions, will run a serious risk of condensation in the enclosure [5, p. 12]. As a result, the electronics will deteriorate and components may be stressed from the freezing water at subzero degrees. Possible remedies may be potting compounds and drying agents [5, p. 13], but will not be tested at this stage.

Chapter 7

Discussion

7.1 Simulations

The transient simulations in section 5.3.1 give us a basis to compare with a similar case using the former plastic probe, dating back to the fall 2011. For the pure polyolefin design presented in chapter 4, the transient response should be of a similar shape and magnitude seen in the plots of the experimental data (see figure 2.5b, taken from project report 2011 [5, fig 4.3a]) due to the similar insulating casing and thermal boundary conditions as mentioned earlier.

However, to compare the simulation data with the experimental data more easily, we plot them together as seen in figure 7.1. The plots are made for sensor 8, which is one of the more "stable" sensors in the data set; the experiment was conducted with occasional stirring to even out developing temperature gradients in the medium, which led to some stagnations and sudden jumps in the temperature progress.

Looking at figure 7.1, it is evident that the experimental data follows the transient response for the simulation data with $h = 400$ $\mathrm{Wm^{-2}K^{-1}}$, before ultimately stagnating at a non-zero temperature. Assuming the stagnation follows from the temperature gradient in the sample, the simulations appear reasonable for a convective constant around $h = 400$ $\mathrm{Wm^{-2}K^{-1}}$.

The weakness in this comparison follows from the assumption of a homogeneous medium and zero static offset when the plastic probe was calibrated – we have to some degree eradicated sensor differences (through calibration) in the experimental data following from internal heat conduction, whereas the simula-

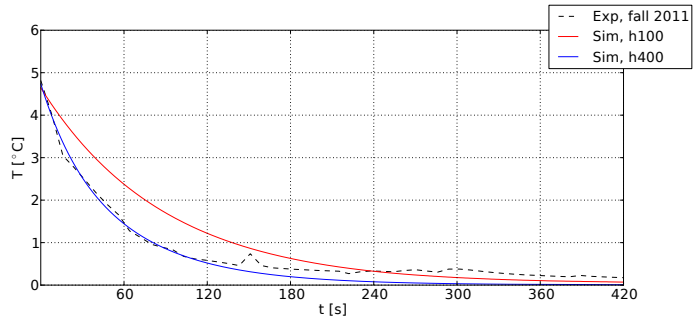

Figure 7.1: Plot of sensor 8 for both the experimental data gathered the fall 2011 with the former plastic probe [5], and the simulated data for the polyolefin design with $h = 100$ and 400 $\mathrm{Wm^{-2}K^{-1}}$. Note that the simulated data is given a negative time shift to counter the different temperature starting point at $t = 0$ s.

tions maintain and certainly highlight such discrepancies between sensors. We can therefore not compare with the experimental offsets [5, fig 4.3b], since we do not know the contributions from the medium's temperature gradient and the inherent heat transport.

Using figure 7.1 to conclude that the experimental data is in accordance with the simulation data when h is around 400 $\mathrm{Wm^{-2}K^{-1}}$ nevertheless, we can stipulate what the improvement would be if we adopt a metal cap design. Going from polyolefin to metal caps, focusing on the high value of h, we see that:

- The temperature time derivative (figure 5.7) is increased by a factor 10 for stainless steel and 20 for brass at $t = 0$ s, but falling within a 5 % difference after a minute.

- The static offset is brought within an acceptable margin for both stainless steel and brass (figure 5.8), surpassing the accuracy requirement for all sensors, as opposed to sensor 1 and 2 for the polyolefin solution. For a small h, the brass peaks at around 2.2 mK, whereas the polyolefin approaches 40 mK.

- Temperature smearing is significantly reduced (by $60-70$ %), with just the nearest neighbours – sensor 6 and 8 – exceeding a 10 mK offset (figure 5.9) at this setup. However, for lower values of h, sensor 5 and 9 are bordering the accuracy limit for the stainless steel caps.

Furthermore, the plots show that the differences between stainless steel versus brass caps are greater for lower coefficients than $h = 400$ $\mathrm{Wm^{-2}K^{-1}}$. Although their thermal properties are far apart, as shown in section 4.2, we have an indication that the metal used for the caps is not the principal limiting factor for the transient response or offset reduction when the heat dissipated/absorbed by the caps is sufficiently large. The impediment caused by e.g. the thermal paste – which is in contact with the sensors, caps and polycarbonate slots – may be an alternative limiting factor for such cases.

Regardless of the type of metal, the simulations indicate that a metal cap solution is superior to a pure polyolefin version, with the cardinal argument being that the polyolefin is unable to keep all sensors within the accuracy requirement. The offset shown in figure 5.8a can only to some extent be reduced through calibration, but as shown in the plot, the offset will vary with the boundary conditions defined by the medium the probe is submerged in – in this case the convective coefficient and temperature of the calibration medium. We have in other words no guarantee that the instrument will fulfill the accuracy requirement in another medium, despite reducing the offsets through calibration. The experimental data highlights this problem, with increasing deviations between sensors when submerging the plastic probe in a medium with another temperature [5, fig 4.4]. However, with the metal caps which evidently have a better thermal contact between sensors and medium, this problem is eliminated by not having the large offset to minimise through calibration.

On the other hand, the difference in crosstalk or smearing may not be as unambiguous as it appears in figure 5.9. Even though the plots indicate a lesser degree of temperature interdependency for the metal cap versions, the pieces of metal may inadvertently contribute to an increase in the heat transport along the longitudinal axis of the probe casing[1], thus altering the temperature gradient of the medium it is submerged in. For the simulations, such implications are neglected when setting a constant temperature for the medium.

7.2 Instrument

Although the development of a new generation of the spatial temperature instrument has come a long way, unforeseen delays and manufacturing difficulties has

[1] In essence, by adding the metal caps, we have inserted 15 sections where the heat transport is increased. The magnitude in the longitudinal direction of the probe will depend on their sizes and implementation, which are decided from a manufacturing perspective – after the simulations were performed.

ultimately resulted in us not being able to present an operational instrument utilising the improved probe at this point.

On a positive note, the metal cap version of suggested probe design described in chapter 4 is almost complete with only the assembly of parts remaining, which indeed was a major concern going into the project: Whether or not it was plausible to produce a probe with our prototyping techniques that ensures a good thermal contact for the sensors, while also retaining the low interference of the previous plastic probe. Although this has yet to be tested, we are close to finalising the assembly for such a metal cap version, and we have a good indication of the performance through the simulations.

The major difference between what is looking to be the final implementation, and the one used in simulations, is the transistion to thin brass films rather than basing the caps on thicker sheets. Although the thermal path is decreased, with conduction through the metal being in inverse ratio to the thickness (see equation (4.1)), the thin film will not distribute the heat as well across its surface area – making the size of the window through the polyolefin tube significant for the thermal performance. How large the impact of that change will be, going from thicker sheets to thin films, has not been investigated. The 150 μm thick films should however not pose the same problem with longitudinal heat conduction as brass sheets of, say, 0.5 mm thickness. Reducing conduction along the probe is paramount, so as not to interfere with the natural temperature gradient in the medium to be examined.

Chapter 8

Conclusion

Accurate spatial temperature measurements has been an expressed wish by ice researchers for years, leading to the start-up of a project to develop an instrument containing a sensor array in 2009. By 2011, the measuring electronics were exceeding the desired accuracy of 0.01°C, but the thermal impacts of the previous sensor probes were too large for the instrument to fulfill this requirement.

The design of, and near completing of, a new probe has been conducted, which not until now should bring the accuracy within the designated 0.01°C. This claim has not been verified through experiments as of yet – not having reached an operable state for the revised instrument – but is instead backed up by simulations utilising a simplified model of the refined design. Such simulations rely nevertheless on adjustments according to corresponding experimental data, and can for the time being not be considered as verification of its thermal performance.

Two suggestions are presented for the design, both cylindrical in shape and a casing based on the same insulating polyolefin tubing from an earlier version. The most complex of the two, the one which is nearly completed, features windows at the sensor locations, with conductive brass films covering the sensors.

Simulations indicate that a probe with a purely insulating casing will not be able to guarantee sufficient accuracy, with the temperatures at the sensors being dependent on their positions. Their static offsets can approach $0.03 - 0.04$°C, depending on the medium and boundary conditions, thus exceeding the acceptable limit. Furthermore, the insulating casing induces a significant crosstalk, i.e. an interdependency between sensors that will lead to an artificial smearing when measuring a temperature gradient.

The static offset and crosstalk are greatly reduced when using conductive

brass caps over the sensors, with simulations indicating that all sensors fall comfortably within the 0.01°C range – peaking at 2.2 mK – and the effect of crosstalk is reduced by around 60 – 70 % between neighbouring sensors for the cases that are simulated.

When the new generation of the instrument is assembled and in an operative state, acquisition of experimental data should follow so as to check whether the simulation data is representative for the new probe design. Even then there are a few aspects left before concluding the development, including e.g. calibration and the incorporation of wireless communication.

References

[1] Egil Wille. Measurement and logging of ice temperatures. Project report, Norwegian University of Science and Technology, 2009.

[2] Egil Wille. Measurement and logging of ice temperatures. Master's thesis, Norwegian University of Science and Technology, 2010.

[3] Anders Lund Eide. Take part in work to develop, document and verify equipment for calorimetric testing of ice with different salt content levels. Master's thesis, Norwegian University of Science and Technology, 2011.

[4] Innovative Sensor Technology. Platinum temperature sensors. URL: `http://www.ist-ag.com/`. Note: Product series 6W, type 232, 100 Ω.

[5] Karsten Meyer. On the design of accurate spatial and temporal temperature measurements in sea ice. Project report, Norwegian University of Science and Technology, 2011.

[6] ITW Chemtronics. CircuitWorks Boron Nitride Heat Sink Grease. Technical datasheet at URL: `http://www.chemtronics.com/products/americas/TDS/CW7250TDS.pdf` – MSDS at URL: `http://www.chemtronics.com/products/americas/MSDS/7250.pdf`.

[7] The Engineering ToolBox. URL: `http://www.engineeringtoolbox.com/`.

[8] Interconnecting and Packaging Electronic Circuits. IPC-2221 Generic Standard on Printed Board Design, 1998. Figure 6-4 Conductor thickness and width for internal and external layers.

[9] Harwin. M40-620xxxx Customer Information Sheet. URL: `http://www.harwin.com/include/downloads/drawings/M40-620.PDF`.

[10] Frank P. Incropera, David P. Dewitt, Theodore L. Bergman, and Adrienne S. Lavine. *Fundamentals of Heat Transfer*. John Wiley & Sons, 6th edition, 2007.

[11] William H. Press, Saul Teukolsky, William T. Vetterling, and Brian P. Flannery. *Numerical Recipes*, pages 1043–1053. Cambridge University Press, 3rd edition, 2007.

[12] ANSYS, Inc. ANSYS Mechanical APDL Thermal Analysis Guide, November 2011. Release 14.0.

[13] Ronald E. Walpole, Raymond H. Myers, Sharon L. Myers, and Keying Ye. *Probability & Statistics for Engineers & Scientists*, pages 407–409. Pearson Education International, 8th edition, 2007.

[14] TE Connectivity. RAYCHEM Tubing Products. URL: `http://www.te.com/`. Part Number: SST-48-07/226.

[15] 3M. Polyimide Film Tape 5413. URL: `http://www.3m.com/`.

[16] Hammond Manufacturing. 1555 "F" Series. URL: `www.hammondmfg.com/1555F_SL.htm`.